Taxanes Hybrid Nanovectors: From Design to Physico-Chemical Evaluation of Docetaxel and Paclitaxel Gold (III)-PEGylated Complex Nanocarriers

Gwendolyn Marguerit, Hanane Moustaoui, Maroua Ben Haddada, Nadia Djaker, Marc Lamy de La Chapelle, Jolanda Spadavecchia

WILEY-VCH

DOI: 10.1002/((please add manuscript number))
Article type: (**Full Paper**)

Taxanes Hybrid Nanovectors: From design to physico-chemical evaluation of docetaxel and paclitaxel gold (III)-PEGylated complex –nanocarriers.

Gwendolyn Marguerit[1‡], Hanane Moustaoui[1], [‡]Maroua Ben Haddada[1], Nadia Djaker[1], Marc Lamy de la Chapelle[1], Jolanda Spadavecchia[1*]

[1] *CNRS, UMR 7244, CSPBAT, Laboratoire de Chimie, Structures et Propriétés de Biomateriaux et d'Agents Therapeutiques Université Paris 13, Sorbonne Paris Cité, Bobigny, France*

[2]*Southwest Hospital, Third Military Medical University, Chongqing, China*

[*] Corresponding author: jolanda.spadavecchia@univ-paris13.fr

ABSTRACT

This study gives an original methodology to synthetize novel metallo-drugs nanoparticles relevant for medicinal chemistry. Gold ($HAuCl_4$) are complexes with antitumor compounds (paclitaxel (PTX); docetaxel (DTX)) and dicarboxylic acid-terminated polyethylene-glycol (PEG) that plays a role of surfactants. The proposed synthesis is fast and leads to hybrid-metal nanoparticles (AuNPs) in which drug solubility was improved. The interactions between drugs (DTX; PTX), PEG diacid (PEG) and Au (III) ions to form hybrid nanocarriers called DTX IN PEG-AuNPs and PTX IN PEG-AuNPs, were characterized by various analytical techniques (Raman and UV-Vis spectroscopies) and transmission electron microscopy(TEM). The efficient drugs release under pH conditions were also achieved and characterized showing an amazing reversible equilibrium between Au (III)-complex-drug and Au^0NPs. For therapeutic purposes, such AuNPs were then decorated with the anti-EGFR polyclonal antibodies, which specifically recognizes the hERG1 channel aberrantly expressed on the membrane of human lung cancer cells. This paper, through an original chemical approach, will occupy an important position in the field of Nanomedicine, and hope that novel perspectives will be proposed for the development of high drug-loading nanomedicines.

KEYWORDS: AuNPs, Docetaxel, Paclitaxel, Raman Spectroscopy, goldcomplex, nanomedicine, nanovector.

1. Introduction

The development of new nanotherapeutic agents is one of the main challenges in the field of nanomedicine [1],[2],[3]. The study of the structure-activity relationships (SAR) of synthetic drug analogs paves the way to develop new nanovectors for which their chemical-physical properties are very critical in cell biology studies[4]. An ideal nanovector consists in a drug or a biomolecule embedded in or grafted on nanoparticles or porous nanomaterials capable to recognize specific cells (cancer cells for instance) [1, 5] in order to improve pharmacokinetics and biodistribution phenomena, with consequent reduction of systemic side effect. The current objective in nanomedecine is to develop protocols for the synthesis without toxic chemicals of biodegradable and biocompatible nanoparticles. Nanovectors alias "nanomedicines" can prevent several drawbacks of free drugs, such as poor water solubility, low drug-loading (generally less than 10%), and short drug half-life in vivo [6],[7]. Numerous nanovectors have been designed, synthesized and tested, but only a few encapsulated forms of anticancer drugs have been marketed[8],[9].Gold nanoparticles (AuNPs)[3, 10] are presented as a very good candidates for drug vectorization and targeting since they allow the constitution of dendrimers of several types and size, they can be easily modified with various ligands such as poly(ethylene-glycol) PEG), they can be functionalized with targeting moieties [5a] [11] ,.Anticancer drug can be covalently attached to the AuNP as proposed by Gibson et al. for a paclitaxel derivative[12] and by Prabaharan et al. for doxorubicin[13],[13a]. Entrapment of the drug without covalent binding to the AuNP appears to be simpler and may facilitate uptake of the drug by the cancer cell, as opposed to endocytosis of the whole AuNP, a slower and less efficient process[14].

Taxanes have been recognized as a family of very efficient anticancer drugs. The two main taxanes are Taxol for paclitaxel (PTX) and Taxotere for docetaxel (DTX). The antitumor mechanism of action for DTX and PTX is the hyperstabilization of microtubules that binds β

subunit protein of tubulin inhibiting their depolymerization. However, the formulation in use has shown dramatic side effects[12] as their poor water solubility is responsible of drug delivery problems and consequently of systemic toxicity that limited their clinical application. The use of nanoparticles for taxanes delivery can improve their water solubility minimizing the side effects and increasing the tumor-targeting distribution[15].Recently H.Moustaoui et al. have designed a new nano-therapeutic agent based on a gold-doxorubicin complex called DOX-IN-PEG-AuNPs[16]. In this nanovector, doxorubicin (DOX) molecules and PEG diacide molecules were chelated with Au (III) ions from tetrachloroauric acid ($HAuC_{l_4}$). It was demonstrated that effective DOX release was carried out at pH 4, with stability attained at AuNP diameter close to 20 nm in physiological pH. This strategy can be applied to any drugs possessing complexation ability, such as carboxylates, phosphonates, including anthracycline, alkaloid and flavonoid[16],[17],[18],[19],[20].The particle size and pH-responsive point of nano-therapeutics are dependent on the complex combinations of polymer ligands, drug molecules, and center metal ions[18]. The purpose of this study is to provide novel nanomedicines for biological applications by using taxanes (DTX or PTX) complexed to gold ions to build nanoparticles (DTX IN PEG-AuNPs; PTX-IN PEG-AuNPs), with different chemical–physical properties to improve their biological activity. Chemical-physical characterizations were performed to demonstrate the change of taxanes conformation during the formation of the AuNP and the drug release from the gold nanocarriers. We envision that this study will occupy an important position in the field of Nanomedicine, and hope that novel perspectives will be proposed for the development of high drug-loading nanomedicines. To the best of our knowledge, these aspects have never been described before in published reports.

2. RESULTS AND DISCUSSION

Formation mechanism of DTX IN-PEG-AuNPs and PTX IN-PEG-AuNPs

Previously H.Moustaouiet al.have designed a new nano-therapeutic agent based on a gold-doxorubicin complex called DOX-IN-PEG-AuNPs [16]. Chemical-physical characterizations and biological "*in vitro*" studies, have fully elucidating that, the change of doxorubicin (DOX) conformation during the formation of gold-nanostructure by complexation have a large influence in its therapeutic activity. Other authors have studied the mechanism of hybrid nanoparticles and competition effect with different capping agent on the growth process[21].

The purpose of this study is to demonstrate the formation of stable complexes of PEGylated Au(III)-DTX and PEGylated Au(III)-PTX respectively as building blocks of gold nanoparticles. The main difference with previously reported synthetic procedures is that both PTX or DTX participate to the stabilisation of AuNPs *via* complexation between their chetone and hydroxyl groups with chloride auric ions. In our case, the formation of gold NPs from $AuCl_4^-$ includes some mains steps (**scheme 1**):

(1) Complexation of DTX-$AuCl_4^-$or PTX-$AuCl_4^-$ and generation of gold clusters.

(2) Initial reduction of drug-metal ions by dicarboxylic acid-terminated PEG that adsorbs onto DTX-Au or PTX-Au complexes;

(3) Reduction of metal ions in that vicinity and growth of gold particles and colloidal stabilization by molecules of PEG polymers.

In the first step, DTX and PTX were added in $HAuCl_4$ aqueous solution to complex with him. Thus, the positively charged of PTX or DTX in water solutions shows strong electrostatic interaction with negatively charged $AuCl_4^-$ions and they form a complex PTX-$AuCl_4^-$orDTX-$AuCl_4^-$,that plays a final role in growth process of NPs. The addition of PEG-COOH increases the kinetics of reduction by complexation of Au ions[5b], controlling the growth process of nanoparticles (second step). Finally, the reduction by $NaBH_4$, refine the grow process of nanoparticles (third step). **The quantum yield of obtained drug-nanoparticles was 83% for DTX IN-PEG-AuNPs and 76% for PTX IN-PEG-AuNPs respectively**. All products of our synthetic procedure **showed high stability (Stability test- Supporting Informations) and**

were extensively characterized by UV-Vis absorption spectroscopy, TEM and Raman Spectroscopy.

Comparative physico-chemical characterization of DTX IN-PEG-AuNPs and PTX IN-PEG-AuNPs:

DTX (Taxotere) and PTX (Taxol) are chemical taxanes analogs except two groups in the chemical structure[22],[12]. The differences are highlighted by the red groups. In particular, DTX shows a hydroxyl functional group on carbon 10 and a tert-butyl carbamate ester on the phenylpropionate side chain while PTX has an acetate ester and a benzamide[22],[12].DTX is more water soluble than PTX due to its chemical structure[7b]. In previous studies, DTX and PTX were derivatized at the hydroxyl group in the C-2' position to form an derivatized acid ester[23].The free hydroxyl group in this position is essential for anticancer activity[24].In our study, PTX and DTX were complexed to the $AuCl_4^-$ solution, in order to form metallo-micelles as described previously[16]. The addition of diacid polymer molecules (PEG-COOH) in the mixture involve the initial reduction process during the nucleation and growth process determining the final shape and size of the nanoparticles controlled by the concentration ratio between the gold salt and the different capping drugs. TEM images of PTX IN-PEG-AuNPs show a well dispersion of the nanoparticles with an average size of 20 ± 1nm (**Figure 1-A)**. Different nanostructures were obtained with DTX IN-PEG-AuNPs. They display a snow-like shape, embedded in a shell of PEG, with a similar diameter around 22±1nm (**Figure 1-B**).Other authors have reported the synthesis of similar nanostructures using dicarboxylic PEG[16], while another group has produced snowflakes nanoparticles by incorporating protoporphyrin molecules in the growth solution of AuNPs. Based on previously reported findings [16, 21b, 25], we suppose that, when DTX and dicarboxylic PEG were added to the $AuCl_4^-$ solution, the PEG was bound initially to Au (III) in a mushroom conformation followed by a conformational change to brush mode.

The absorption spectra of PTX IN-PEG-AuNPs and DTX IN-PEG AuNPs were characterized by a small peak at 300 nm, assigned to the PTX or DTX absorption, and a surface plasmon band at 535 nm(**Figure 1-C blue line)** and 533 nm (**Figure 1-C red line)** respectively. PEG-COOH can be used as stabilizing polymers for AuNPs due to the formation of coordination bands between the Au ions and the chetone or the carboxylic groups of PTX or DTX respectively. This chelation induces a better dispersion of the Au ions, which were easier reduced to form single AuNPs of relatively uniform size.This behavior is associated to π-π^* electronic transitions due to interactions between the taxanesring and $AuCl_4^-$ ions[25] giving clear evidence of the complex formation. The loading of DTX on the gold nanoparticles (DTX IN PEG AuNPs) was confirmedby the strong decrease of the band at 530 nm and an increase of band at 300 nm in the UV-Visible absorbance (**Figure 1-C red line)** and the tendency of snow-like shape to agglomerate differently to PTX IN-PEG-AuNPs. This chemical behavior is due to a different adsorption onto gold facets [110] of PTX and DTX, based on their different steric conformation of chemical groups during nucleation and growth process of AuNPs . In addition the color bright pink-violet of both nanoparticles and the UV-Vis spectra remain unalterated after storage for more than six months at room temperature suggesting the formation of stable particle suspension.The NP sizes were confirmed by DLS measurements (**Table 1**). The gold surface saturation was achieved at a PEG addition concentration of 18.2 μg/ml, as described previously[16], that corresponds to approximately 1.20 dicarboxylic PEG molecules/AuNP. Zeta potential measurements show that PTX IN-PEG-AuNPs and DTX IN-PEG-AuNPs were colloidally stable at physiological pH (z-potential = -29 ±1 mV and -30 ±1 mV with a PdI equal to 0.3) (**Table 1**). This stability was enhanced with the presence of the PEG coating[16].

Table 1: z-potential and hydrodynamic diameter of PTX IN PEG-AuNPs and DTX PEG-AuNPs.

Synthetic product	Zeta potential (mV)	Hydrodynamic diameter (nm)	PdI
PTX IN PEG-AuNPs	-29 ± 4	20 ± 2	0.3
DTX IN PEG-AuNPs	-30 ± 1	22± 2	0.3

The steric arrangement of PTX and DTX during synthetic process of pegylated gold nanoparticles was confirmed by Raman spectroscopic analysis (**Figure 1-D**).T.S Renuga Devi et al.have studied and characterized PTX-polymeric nanoparticles by FT-IR and Raman spectroscopies [26].These spectroscopic analysis showed that the specific functional groups of the PTX-polymeric nanoparticle have the same chemical characteristics than the pure paclitaxel drug, indicating that the molecular interaction with the NP surface does not affect the chemical structure of the drug[23],[26]. Contrary to this study, even if we have involved similar ingredients (drug, polymer) chelated to gold ions in order to form gold nanoparticles, the spectroscopical fingerprints of our final nano-drug are not peculiar compared to the *free* drugs.

In detail, Raman spectra of free PTX and DTX and PTX IN-PEG-AuNPs and DTX IN-PEG-AuNPs in water exhibit many bands in the region 500-2000 cm^{-1} (**Figure 1-D**). More details on the band assignment are given in the table S1 on the supporting information (The wide band observed around 1600 cm^{-1} on the PTX IN-PEG-AuNPs and DTX IN-PEG-AuNPs Raman spectra is assigned to the water). The free PTX and DTX Raman spectra are very close since both molecules are very similar and as a consequence show the same vibrational modes. The same observation can be done for the PTX IN-PEG-AuNPs and DTX IN-PEG-AuNPs Raman spectra. This means that the PTX and DTX have similar structure in interaction with the gold surface. However, large differences are observed between the free PTX or DTX and when they are interacting with the AuNPs. Only few bands remain as the two bands around

1000 cm^{-1} and the one around 1620 cm^{-1}. The other ones are less intense or completely disappeared. For instance, the strong band at 1712 cm^{-1} assigned to C=O carbonyl stretching of nalidixic acid[27] disappears after formation of gold nanoparticles. Such spectral modifications are relevant of the steric conformational change of the drugs after grafting on the gold nanoparticles. On the PTX IN-PEG-AuNPs and DTX IN-PEG-AuNPs Raman spectra new bands also appear as an intense doublet at 720-760 cm^{-1} due to C-H plane deformation and a strong peak at 1439 cm^{-1} assigned to ν C-C stretching. These bands are due to variation of the steric conformation of the drug, and become more prominent upon complexation, as described previously[28],[16].As matter of fact, when C=O and hydroxyl groups of DTX and PTX interacts with a metal, the steric conformation becomes more tilted in respect to the planar one[16, 28].

Focusing our attention on the spectral range 200-500 cm^{-1}**(Figure 2A)**, and 2000-3100 cm^{-1}**(Figure 2 B)**, one can detect several spectral changes which confirms a chemical and steric modification of each drug (PTX;DTX) after complexation with gold ions and PEG-diacide molecules. One of the Raman fingerprint of the DTX IN-PEG-AuNPs is the presence of a band around 263 cm^{-1} whereas for PTX IN-PEG-AuNPs, double peak at 235-285 $cm^{-1}$is observed **(Figure 2A)**.These bands can be assigned to the gold chloride stretches, ν (AuCl), and δ (OAuO) in aliphatic ring (C7-C9), and is a clear evidence of the formation of a complex between $AuCl_2^-$ and DTX or PTX in solution. Furthermore the presence of double peak for DTX compared to a single peak for PTX confirmed the distinct chemical behaviour of these analogue drugs, under complexation with gold ions, probably due to the differences in their chemical groups. The common peak at 430 cm^{-1} is due to the vibrations δ(OH…O), ν(OH…O) of the PEG. Based on the spectrochemical and previously theoretical results, we assumed that Au^{3+} ions promoted the deprotonation of the DTX and PTX cicloexhanol group at position C7 and C9.The bands exhibited in the region 3000 cm^{-1} can be assigned to aromatic C-H stretching[29],[30] **(Figure 2B).** In particular, the peak at 3060 cm^{-1}, was used for

selective imaging of PTX *drug*[31],[29]. However, the vibrational frequencies exhibited at 2946-2952 cm^{-1}, are considered to be due to C-H stretching vibration of the compounds (**Table S1** in the **Supporting Information)**. These peaks disappeared after formation of drug-nanoparticles (PTX IN PEG-AuNPs; DTX IN PEG-AuNPs), while a broad band composed of several peaks appears in the spectral range 2850-2930 for both nanovectors due to the symmetric CH_2-CH_3 stretch vibration of PEG-diacide molecules confirming the main role of the polymer in the synthesis of the nanovector.

Drug loading and release of DTX IN-PEG-AuNPs and PTX IN-PEG-AuNPs:

The solubility of DTX and PTX in water is very poor (3-6µg/mL^{-1})[11a]. Astruc et al have improved the solubility of DTX by encapsulation in pegylated gold nanoparticles using click chemistry under several steps[11a].Recently, other authors have studied the process of co-loading of Curcumin and PTX onto Polymer-functionalized Reduced Graphene Oxide to pick up the PTX efficiency loading of about 98% in the presence of Curcumine and polymer[32].In our case, upon complexation of $AuCl_4^-$ and encapsulation into PEG diacid chaines, the DTX and PTX molecules reside inside the AuNP core[16]. The successful loading ratio of PTX and DTX into PEG-AuNPs, were evidenced by the characteristic absorption peaks at 260nm from PTX and DTX **(Figure S3-a-b)**. The standard absorption of PTX and DTX were plotted in the inset of figure **(Figure S3-c)**, according to UV-Vis absorbance spectra of PTX and DTX at various concentrations. The loading efficiencies were estimated to be 86% for DTX and 85 % for PTX, with 8.3 µg and 8.1µgof DTX and PTX present in 2.6×10^{-7} mol of NPs (data not shown).DTX and PTX releases were pH- and time-dependent (**Figure 3 A-B**). A sustained drug release was observed in the first 5 h for both drugs at pH 4 and 7, which is highly favorable for drug delivery as the cancer cells thrive in acidic conditions. **Similar results were observed at pH 5 and pH 6 under some conditions (Figure S4).** We supposed that the release of DTX and PTX were controlled by a dynamic equilibrium between Au (III)-drug

complexes trapped into AuNPs by the hydrophobic interactions between PEG and drugs. As previously described, the mechanism by which acidic pH triggers drug release is probably associated to the presence of carboxylate groups in the chemical structure of PEG molecules[16]. Such groups become protonated at acidic pH. This reduces the electrostatic interactions occurring between PEG and drugs that stabilize the DTX IN-PEG-AuNPs or PTX IN-PEG-AuNPs structure.

We suppose that, the ionic strength and protonation of DTX and PTX into PEG chains improve the water solubility of the drug molecules, taking advantage of the drug release from AuNPs. Indeed, a remarkable moiety of DTX and PTX in the dissociated complex are released, with consequently particle conformational change, due to the PEG chain and diffusion phenomena[5b, 16].

Drug release and Effect of the pH on Raman spectra

In order to better understand the intrinsic differences between these two nanomedicine candidates, comparative Raman studies were carried out at pH 7.0 and 4.0 in order to follow the PTX and DTX release under a range time(from 1h to 96h) (**Figures S1-A and S2-A in Supporting Informations**). Previously other authors have demonstrated spectroscopical differences and variation of chemical conformation during drug release profiles[16, 18, 25]. Thus, PTX IN-PEG-AuNPs and DTX IN-PEG-AuNPs were characterized by Raman spectroscopy after incubation for 96 h in PBS at 37 °C in order to (1) confirm the drug release and (2) to evaluate variations in the chemical orientation of PTX and DTX at pH 4.0 (when PTX and DTX are protonated) and pH 7.0 (when PTX and DTX are partially deprotonated). The Raman band at 263 cm^{-1} and 235-282 cm^{-1} were monitored to evaluate the PTX and DTX release, respectively, from AuNPs[16, 28] (**Figure S1-B –S2-B in Supporting Informations**). The intensity of this band continuously decreased overtime, until completely disappearing after 96 h (**Figure 4-5 panel A**). Besides, a strong Raman intensity decrease was observed in the spectral range 2600-3000 cm^{-1} and 200-400 cm^{-1}, confirming that, DTX and PTX release

were pH- and time- dependent. At both pH we observed that after 96 h**,** the Raman spectra, are dominated by the water mode at 1637 cm^{-1} and the PEG Raman spectrum[16]. The DTX and PTX spectrum observed in DTX IN-PEG-AuNPs and PTX IN-PEG-AuNPs are largely reduced (**Figure S1-S2 A-B in Supporting Informations**).We monitored our experiments each hour, noting a remarkable spectral change at 96h, beginning at time 5h.We also observed an original morphological variation of our nanovectors under pH 4.0 and 7.0. (**Figure 4-5 panel B**).Specially for DTX IN PEG-AuNPs, we observe a gradual change of shape and size from nanoflowers of about 20 nm (as synthetized) to small nanospheres of about 2-3nm (pH 4.0).Between these two states, we observe an intermediate one(pH 7.0) in which a morphological change as well as a depolymerization from the original structure was more evident (**Figure 4 B**).Besides PTX IN PEG-AuNPs appears to be embedded in globular clusters (pH 7.0), that change again in polymeric gold-sphere at pH 4.0 (**Figure 4 B**). As mentioned previously, the pH value plays a key role during the reduction process of Au (III) to Au^0, in the formation of gold nanoparticles[33]. In particular, S.Yang et al have demonstrated that citric acid, forms complexes with Au (III), at various pH values, influencing the particle size[33]. In our case, PEG diacide, like citric acid, influences the formation of complexes PEG-Au (III)-DRUG, during growth of NPs[16, 34]. We conclude that, under pH conditions, a dramatic change of shape and size of DTX PEG-AuNPs and PTX PEG-AuNPs were made and PTX and DTX were released as gold complex, as previously described for other drugs [16].

Drug release and effect of the pH on localized surface plasmon (LSP):

Similar release experiments were also observed by LSP monitoring. **Figure 6 (A-B)** shows LSP resonance spectra before and after incubation of nanoparticles under specific conditions (pH: 4.0-7.0; time: 96 h; **T: 37 °C**). In the case of PTX IN PEG-AuNPs (**Figure 5 panel A**), after 96 h, at pH 7, we observe a disappearance of the LSP band at 535 nm and the peak at

310 nm due to the PEG-$AuCl_2^-$. An increase of the peak intensity at 256 nm probably due to PTX fingerprint associated to $AuCl_2$ ions upon complexation was observed. This increase occurs at pH 4, confirming the complete release of the PTX drug. A different behavior is observed in the case of DTX IN PEG-AuNPs (**Figure 6 panel B**), in which after incubation at pH 7 for 96 h, we observe a disappearance of LSP band at 535 nm, while the band at 310 nm remains unchanged confirming the presence of the PEG-$AuCl_2$. A similar increase of the peak corresponding to DTX drug was observed. At pH 4 under the some conditions, a disappearence of the peak at 310 nm was observed with an enhancement of the peak at 256 nm probably due to DTX-$AuCl_2^-$. This spectroscopical behaviour during pH-drug-release gives evidence of the change of conformation of the drug when it is encapsulated into gold nanoparticles. We assume that during incubation at pH 7 and 4, the drug migrates in the PEG chains and is released upon Drug-PEG-$AuCl_2^-$.This hypothesis can explain a depolymerization and the change of size observed at different pH**.** As described in literature[35], the UV absorption at 304 nm is due to the ligand metal charge transfer (LMCT) bands of $AuCl_4^-$ ions between gold and chloride ligands[36]. After $NaBH_4$ reduction, the LMCT bands of $AuCl_4^-$, decreased dramatically, suggesting that Au^{3+} ions in $HAuCl_4$ solution, were effectively reduced into the metallic state[37]. We can emphasize that during the release at pH 4 and 7, at **T 37°C**, the intensity decrease of the plasmon peak with the increase of the peak at 256 nm of DTX and PTX, is due to reversible equilibrium between AuNPs and DRUG-$AuCl_2^-$. This reversible equilibrium of drug-gold ion as complex at different pH was confirmed by LC-MS and ICP-MS analysis (data no shown).

Active Targeting

Drug-gold nanoparticles (PTX IN PEG-AuNPs; DTX IN PEG-AuNPs) were used as a support for the conjugation of the targeting moiety (anti-EGFR-pAb). The anti-EGFR (epidermal growth factor receptor) binds to the extracellular domain of EGFR in its inactive state and demonstrates activity in a variety of tumor types and in particular lung cancer[38].They

compete for receptor binding by occluding the ligand-binding region, and thereby block ligand-induced EGFR tyrosine kinase activation[39]. Anti-EGFR-pAb molecules were immobilized on the surface of activated nanoparticles through the formation of amide links between the COOH groups decorating the surface of the drug-gold nanoparticles and the NH_2 groups of the pAb (scheme 2).

The interaction between anti-EGFR-pAb and drug-gold nanoparticles were monitored by detecting changes in the LSP band (**Figure 7).** PTX IN PEG-AuNPs showed an LSP band centered at ~530 nm, typical of AuNPs. After immobilization of anti EGFR-pAb onto PTX IN PEG-AuNPs, the resulting solution was colorless and was characterized by a broad LSP peak at 572 nm, which could be assigned to a change of localized refractive index of PEG-AuNPs and to the formation of NP agglomeration. Similar behaviour was observed for DTX IN AuPEG NPs, for which, we observe a broadening of the plasmon band and a red shift from 532 nm to 580 nm after bioconjugation[40]. Based on the UV–Vis spectra, we suggest that such red shift could be associated to the successful bioconjugation of the AuNPs surface with anti EGFR-pAb and the subsequent AuNPs agglomeration associated to the formation of classical van der Waals inter-protein interactions[5a, 41].**All nanoparticles were *free* endotoxin and suitable for further nanomedicine applications.**

3. Conclusions

The success of this study was to provide the design, the synthesis and the characterization of new oncological nanotherapeutics based on stable Au (III)-taxanes complex. We showed that taxanes chemical analogs, such as DTX and PTX reacts skillfully under pegylated gold complexation with an improvement of their solubility and specific release behaviour. The obtained“nanomedicines” showed several favorable advantages as nanotherapeutic for cancer therapy, including (i) solubility and high drug loading; (ii) specific release under pH conditions (iii) over 6-months stability in aqueous solution, and (iv) active targeted ability.

We demonstrated that the Raman technique coupled to LSP monitoring were able to characterize the equilibrium of drug released from gold-complex nanocarriers under acidic and neutral conditions. These results and speculations highlight the potential of the SERS approach to study DTX and PTX–gold interactions in relation to drug delivery and drug biological activity. Further studies are still envisaged, focused on assessing the *in vitro* and *in vivo* assessment toxicity, pharmacokinetics and dynamics on relevant lung-cancer model.

4. Materials and methods

All chemicals were reagent grade or higher and were used as received unless otherwise specified.Tetrachloroauric acid ($HAuCl_4*H_2O$), sodium borohydride ($NaBH_4$), *N*-hydroxysuccinimide (NHS), 1-(3-dimethylaminopropyl)-N'-ethylcarbodiimide hydrochloride (EDC), dicarboxylic PolyEthylene Glycol (PEG)-600 (PEG), phosphate buffered saline (PBS, 0.1 M, pH 7.0, pH 4.0, pH 9.0), Docetaxel (98%), Paclitaxel (98%) were purchased from Sigma Aldrich

Synthesis of DTX IN-PEG-AuNPs

The main steps of synthesis of DTX IN-PEG-AuNPs colloids are described in Scheme 1. 20 ml $HAuCl_4$ aqueous solution (2.5×10^{-4} M) was added to DTX (5 ml, 1.72 x 10^{-4} M in water) and aged for 10 min. 250 µl of dicarboxylic PEG was then added and mixed by magnetic stirring for 10 min at room temperature. Finally, 6 ml of aqueous 0.01 M $NaBH_4$ was added at once. The formation of the DTX IN-PEG-AuNPs was observed as an instantaneous colour change of the solution from pale yellow to bright pink-violet after addition of the reducing agent. Products of each synthetic step were stored at 27-29 °C and characterized by UV-Vis spectroscopy, Transmission Electron Microscopy, and Raman spectroscopy. The "as-prepared" DTX IN-PEG-AuNPs solution was centrifuged at 9,000 rpm for 10 min for three times; then, the supernatant was discarded. The residue was re-dispersed in an equivalent amount of PBS (pH = 7). This was repeated twice to remove excess of not-conjugated dicarboxylic PEG.

Synthesis of PTX IN-PEG-AuNPs

Synthesis of PTX IN-PEG-AuNPs (Scheme 1) colloids were carried out in the same conditions described above for DTX.

Stability of DTX (PTX) IN-PEG-AuNPs as function of pH

The stability of nanoparticles was detected by UV VIS. DTX (PTX) IN-PEG-AuNPs nanoparticles were dissolved in PBS solution 0.1M at different pH (pH 1.68, 7, 12) during 18h (Supporting Informations).

Anti-EGFR-pAb immobilization onto DTX IN-PEG-AuNPs and PTX IN-PEG-AuNPs

The binding of antiEGFR-pAb onto DTX (PTX) IN-PEG-AuNPs surface was performed at pH 9.0 in PBS. Briefly, 20 µl of EDC/NHS (80/20 w/w ratio) aqueous solution was added into 5 ml of DTX(PTX) IN-PEG-AuNPs dispersion.

After 2 h, 50 µL (0.1 ng/ml) of antiEGFR-pAb in PBS was added in 2 ml of the reaction mixture and stirred for 2 h at room temperature. The obtained antiEGFR pAb -DTX(PTX) IN-PEG-AuNPs were centrifuged two times at 9,000 rpm for 10 min to remove excess of not-conjugated anti EGFR-pAb and dried under nitrogen.

Physico-chemical characterization

All the measurements were performed in triplicate in order to validate the reproducibility of the synthetic and analytical procedures.

UV/Vis measurements

Absorption spectra were recorded using a Perkin Elmer Lambda UV/Vis 950 spectrophotometer in plastic cuvettes with an optical path of 10 mm. The wavelength range was 200–900 nm.

Transmission Electron Microscopy (TEM)

All microscopy analysis were realized as previously described [16].

Raman Spectroscopy: The Raman experiments have been performed on an Xplora spectrometer (Horiba Scientifics-France). The Raman spectra have been recorded using an excitation wavelength of 785 nm (diode laser) at room temperature. For measurements in solution, a macro-objective with a focal length of 40 mm (NA = 0.18) was used in backscattering configuration. The achieved spectral resolution is close to 2 cm^{-1}.

Dynamic light scattering (DLS): The size measurements were performed using a Zetasizer Nano ZS (Malvern Instruments, Malvern, UK) equipped with a He-Ne laser (633 nm, fixed scattering angle of 173°) at room temperature.

Zeta potential measurements: All measurements were carried out as previously [16].

Drugs loading efficiency: The amount of the drugs (DTX; PTX) incorporated into DTX IN-PEG-AuNPs and PTX IN- PEG-AuNPs were measured by UV-Vis absorption spectroscopy. Absorption at 260 nm was used to extrapolate DTX or PTX concentrations based on a calibration curve (**Figure S3** in the Supporting Information). The Drug loading efficiency was calculated as follows (**Equation 1**):

$$Drugloadingefficiency(\%) = \frac{C_1 - C_2}{C_1} \times 100 \quad \textbf{Equation 1}$$

Where C_1 is the initial drug content and C_2 is the amount of free DTX or PTX in the filtrate after separation of the nanoparticles by ultrafiltration with an Ultrafree MC centrifugal filter units, (30,000 NMWL, Millipore, USA).

Drug release from AuNPs: PTX and DTX releases were evaluated at physiological temperature (37°C). Drug-loaded AuNPs were dispersed at concentration of 1.5×10^{12}particles/ml in 1.0 ml PBS and performed by dialysis as previously described [16]. The

concentration of drug released from AuNPs was expressed as a percentage of the total drug concentration present in the sample **(Equation 2)** and plotted as a function of time.

$$\%\, Drug released = \frac{Concentration of drug released}{Initial drug concentration} \times 100 \textbf{Equation 2}$$

Endotoxin content in Drug-gold nanoparticles:

As routine quality control of the materials prior to biological testing, the Pierce LAL Cromogenic Endotoxin Quantitation kit (Thermoscientific, France) was used to determine the LPS contamination in Drug-gold nanoparticles (DTX IN-PEG-AuNPs; PTX IN-PEG-AuNPs) before and after conjugation with antiEGFR-pAb. The assay was carried out as manufacturer's protocol, and absorbance was measured at 405 nm to detect the yellow chromogenic colour in the presence of endotoxin. Diluitions of standards and drug-gold nanoparticles were prepared in endotoxin-free water. Drug-gold nanoparticles were tested with and without (blank) the presence of LAL chromogenic substrate to determine any interference in the assay due to the optical properties of the nanomaterial itself. Blanks were substracted from the readings of each NPs sample to accurately determine the LPS contamination. Results, are reported in Table 1 as average (n_{test} =2) ± standard deviation. Endotoxin contamination results were kept into account when defining the type of cytotoxic endpoint to be examined.

Table 1. Endotoxin units detected by means of the LAL Chromogenic Endotoxin Quantitation kit (ND = not detectable; >1= above detection limit of the assay).

Sample	Endotoxin Units (EU/ml)
PEG-AuNPs (control)	ND
Anti-EGFRpAb-DTX(PTX)IN-PEG-AuNPs	>1
DTXIN-PEG-AuNPs	ND
PTXIN-PEG-AuNPs	ND
antiEGFRpAb antibody	>1

References:

[1] N. Ahmad, S. Bhatnagar, R. Saxena, D. Iqbal, A. K. Ghosh, R. Dutta, *Materials science & engineering. C, Materials for biological applications* **2017**, *78*, 553-564.

[2] S. A. C. Carabineiro, *Molecules (Basel, Switzerland)* **2017**, *22*.

[3] R. Arvizo, R. Bhattacharya, P. Mukherjee, *Expert opinion on drug delivery* **2010**, *7*, 753-763.

[4] A. S. Paraskar, S. Soni, K. T. Chin, P. Chaudhuri, K. W. Muto, J. Berkowitz, M. W. Handlogten, N. J. Alves, B. Bilgicer, D. M. Dinulescu, R. A. Mashelkar, S. Sengupta, *Proceedings of the National Academy of Sciences* **2010**, *107*, 12435-12440.

[5] aJ. Spadavecchia, D. Movia, C. Moore, C. M. Maguire, H. Moustaoui, S. Casale, Y. Volkov, A. Prina-Mello, *International journal of nanomedicine* **2016**, *11*, 791-822; bI. Capek, *Advances in colloid and interface science* **2017**.

[6] A. Montero, F. Fossella, G. Hortobagyi, V. Valero, *The Lancet Oncology* **2005**, *6*, 229-239.

[7] aB. Nuijen, M. Bouma, J. H. Schellens, J. H. Beijnen, *Invest New Drugs* **2001**, *19*, 143-153; bQ. Tan, X. Liu, X. Fu, Q. Li, J. Dou, G. Zhai, *Expert opinion on drug delivery* **2012**, *9*, 975-990.

[8] G. Apolone, R. Joppi, V. Bertele, S. Garattini, *British Journal of Cancer* **2005**, *93*, 504-509.

[9] S. Jain, D. G. Hirst, J. M. O'Sullivan, *The British Journal of Radiology* **2012**, *85*, 101-113.

[10] E. Boisselier, D. Astruc, *Chemical Society Reviews* **2009**, *38*, 1759-1782.

[11] aA. Francois, A. Laroche, N. Pinaud, L. Salmon, J. Ruiz, J. Robert, D. Astruc, *ChemMedChem* **2011**, *6*, 2003-2008; bA. C. Powell, G. F. Paciotti, S. K. Libutti, *Methods in molecular biology (Clifton, N.J.)* **2010**, *624*, 375-384.

[12] J. D. Gibson, B. P. Khanal, E. R. Zubarev, *Journal of the American Chemical Society* **2007**, *129*, 11653-11661.

[13] aM. Prabaharan, J. J. Grailer, S. Pilla, D. A. Steeber, S. Gong, *Biomaterials* **2009**, *30*, 6065-6075; bM. Prabaharan, J. J. Grailer, S. Pilla, D. A. Steeber, S. Gong, *Biomaterials* **2009**, *30*, 5757-5766.

[14] Y.-J. Gu, J. Cheng, C. W.-Y. Man, W.-T. Wong, S. H. Cheng, *Nanomedicine: Nanotechnology, Biology and Medicine* **2012**, *8*, 204-211.

[15] L. Zhang, N. Zhang, *International journal of nanomedicine* **2013**, *8*, 2927-2941.

[16] H. Moustaoui, D. Movia, N. Dupont, N. Bouchemal, S. Casale, N. Djaker, P. Savarin, A. Prina-Mello, M. L. De la Chapelle, J. Spadavecchia, *ACS applied materials & interfaces* **2016**, *8*, 19946-19957.

[17] aH. Wang, P. Yang, Y. Tian, Z. Zhang, C. Zhao, *Journal of Inorganic Biochemistry* **1997**, *68*, 117-121; bH. N. Ramaswamy, R. T. O'Connor, in *Developments in Applied Spectroscopy: Selected papers from the Twentieth Annual Mid-America Spectroscopy Symposium, Held in Chicago, Illinois, May 12–15, 1969* (Ed.: E. L. Grove), Springer US, Boston, MA, **1995**, pp. 105-112.

[18] S. Shen, Y. Wu, Y. Liu, D. Wu, *International journal of nanomedicine* **2017**, *12*, 4085-4109.

[19] J. W. Taylor, A. McSkimming, M. E. Moret, W. H. Harman, *Angew Chem Int Ed Engl* **2017**.

[20] A. S. Silva, V. D. B. Bonifacio, V. P. Raje, P. S. Branco, P. F. B. Machado, I. J. Correia, A. Aguiar-Ricardo, *RSC Advances* **2015**, *5*, 10733-10738.

[21] aJ. Politi, L. De Stefano, I. Rea, A. M. Gravagnuolo, P. Giardina, C. Methivier, S. Casale, J. Spadavecchia, *Nanotechnology* **2016**, *27*, 195701; bJ. Spadavecchia, E. Apchain, M. Alberic, E. Fontan, I. Reiche, *Angew Chem Int Ed Engl* **2014**, *53*, 8363-8366.

[22] S. J. Clarke, L. P. Rivory, *Clinical Pharmacokinetics* **1999**, *36*, 99-114.

[23] G. F. Paciotti, J. Zhao, S. Cao, P. J. Brodie, L. Tamarkin, M. Huhta, L. D. Myer, J. Friedman, D. G. Kingston, *Bioconjugate chemistry* **2016**, *27*, 2646-2657.

[24] M. L. Miller, I. Ojima, *Chemical record (New York, N.Y.)* **2001**, *1*, 195-211.

[25] S. Link, M. A. El-Sayed, *The Journal of Physical Chemistry B* **1999**, *103*, 8410-8426.

[26] T.S.R. Devi, S. Gayathri, *International Journal of Pharmaceutical Sciences Review and Research* **2010**, *2*, 106-110.

[27] U. Neugebauer, A. Szeghalmi, M. Schmitt, W. Kiefer, J. Popp, U. Holzgrabe, *Spectrochim Acta A Mol Biomol Spectrosc* **2005**, *61*, 1505-1517.
[28] J. Gautier, E. Munnier, L. Douziech-Eyrolles, A. Paillard, P. Dubois, I. Chourpa, *Analyst* **2013**, *138*, 7354-7361.
[29] E. Kang, H. Wang, I. K. Kwon, J. Robinson, K. Park, J. X. Cheng, *Anal Chem* **2006**, *78*, 8036-8043.
[30] G.Socrate, *Wiley NY* **1980**.
[31] E. Kang, J. Robinson, K. Park, J.-X. Cheng, *Journal of controlled release : official journal of the Controlled Release Society* **2007**, *122*, 261-268.
[32] K. Muthoosamy, I. B. Abubakar, R. G. Bai, H.-S. Loh, S. Manickam, **2016**, *6*, 32808.
[33] S. Yang, Y. Wang, Q. Wang, R. Zhang, B. Ding, *Colloids and Surfaces A: Physicochemical and Engineering Aspects* **2007**, *301*, 174-183.
[34] aM. Khafaji, M. Vossoughi, M. R. Hormozi-Nezhad, R. Dinarvand, F. Börrnert, A. Irajizad, **2016**, *6*, 27847; bJ. Spadavecchia, R. Perumal, S. Casale, J.-M. Krafft, C. Methivier, C.-M. Pradier, *Chemical Physics Letters* **2016**, *648*, 182-188.
[35] X. Liang, Z. J. Wang, C. J. Liu, *Nanoscale Res Lett* **2009**, *5*, 124-129.
[36] aJ. C. Garcia-Martinez, R. M. Crooks, *J Am Chem Soc* **2004**, *126*, 16170-16178; bP. He, M. W. Urban, *Biomacromolecules* **2005**, *6*, 1224-1225; cC.-j. Liu, *Nanoscale Research Letters* **2010**, *5*, 124-129.
[37] aX. Liang, Z.-j. Wang, C.-j. Liu, *Nanoscale Research Letters* **2009**, *5*, 124; bC. Li, D. Li, G. Wan, J. Xu, W. Hou, *Nanoscale Research Letters* **2011**, *6*, 440-440.
[38] aD. E. Gerber, *Drug development research* **2008**, *69*, 359-372; bB. A. Chan, B. G. M. Hughes, *Translational Lung Cancer Research* **2015**, *4*, 36-54.
[39] aF. Ciardiello, G. Tortora, *N Engl J Med* **2008**, *358*, 1160-1174; bN. Normanno, C. Bianco, A. De Luca, M. R. Maiello, D. S. Salomon, *Endocr Relat Cancer* **2003**, *10*, 1-21; cJ. Mendelsohn, J. Baselga, *Oncogene* **2000**, *19*, 6550-6565.
[40] aD. R. Hristov, L. Rocks, P. M. Kelly, S. S. Thomas, A. S. Pitek, P. Verderio, E. Mahon, K. A. Dawson, *Scientific reports* **2015**, *5*, 17040; bM. H. Jazayeri, H. Amani, A. A. Pourfatollah, H. Pazoki-Toroudi, B. Sedighimoghaddam, *Sensing and Bio-Sensing Research* **2016**, *9*, 17-22.
[41] K. H. Müller, M. Motskin, A. J. Philpott, A. F. Routh, C. M. Shanahan, M. J. Duer, J. N. Skepper, *Biomaterials* **2014**, *35*, 1074-1088.

Corresponding Author

*jolanda.spadavecchia@univ-paris13.fr

Author Contributions

The manuscript was written through contributions of all authors. All authors have given approval to the final version of the manuscript. ‡These authors contributed equally.

ACKNOWLEDGMENT

This work has been partly performed on the CNanoMat platform of the University Paris 13.

Figures and scheme

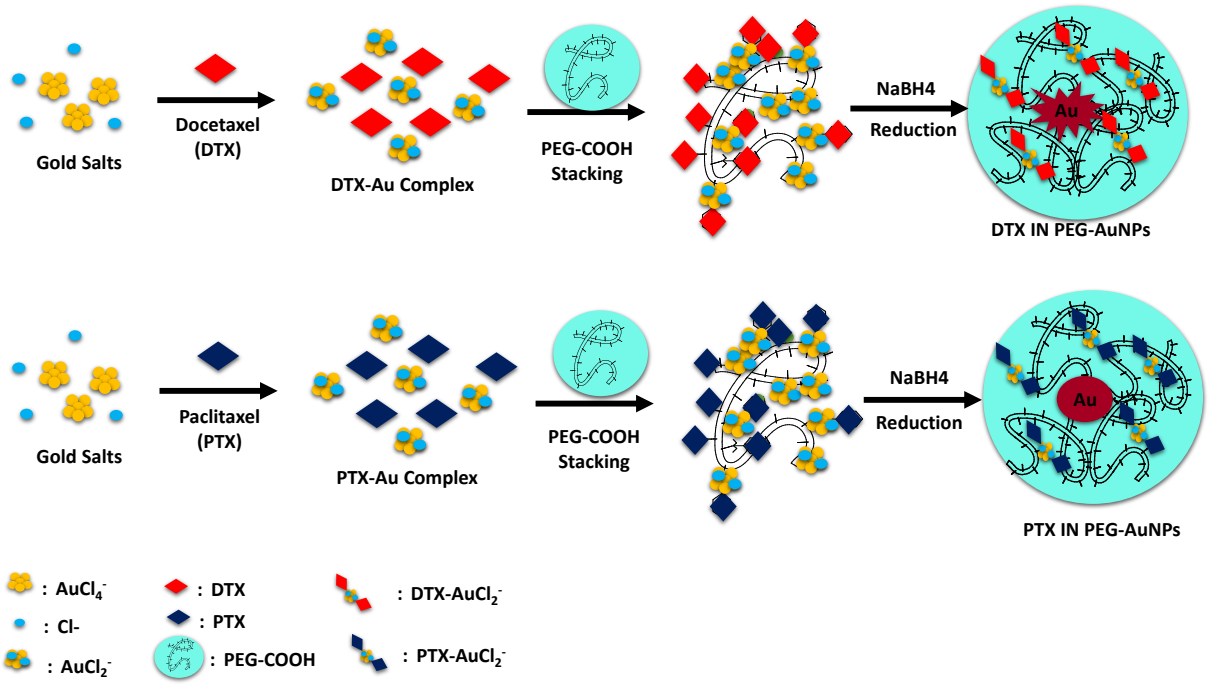

Scheme 1. Schematic representation of the synthesis of DTX IN-PEG-AuNPs and PTX IN-PEG-AuNPs *via* a three-step process (Please note that drawings are not in scale and are not intended to be representative of the full samples composition).

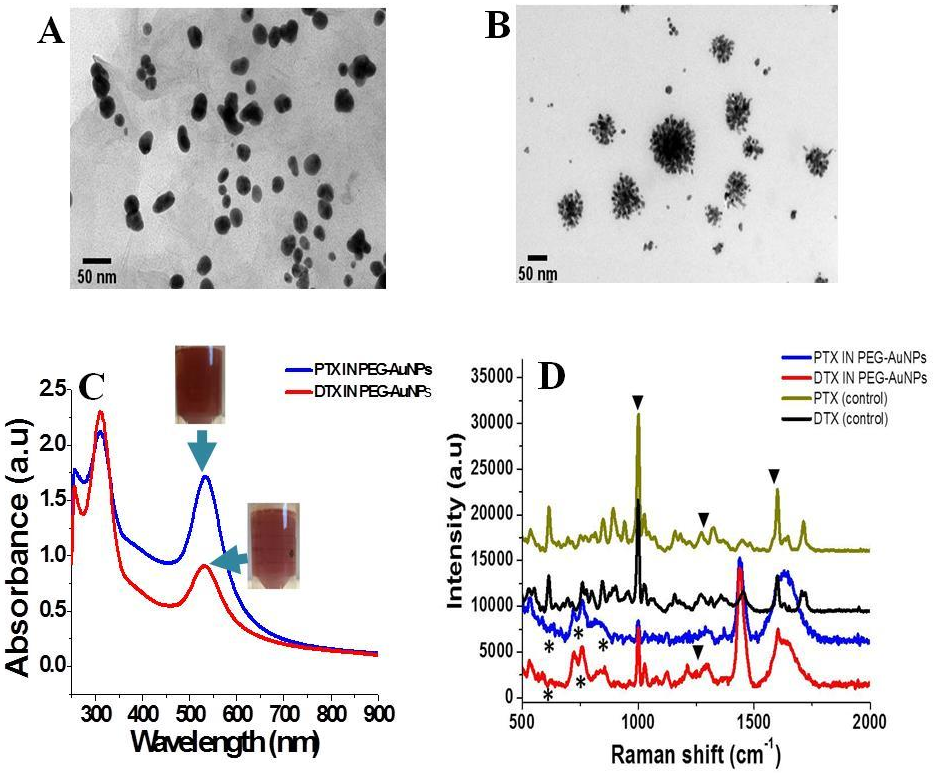

Figure 1. (TEM images of PTX IN PEG-AuNPs (**A**) and DTX IN PEG-AuNPs (**B**); (**C**) normalized UV-Vis absorption and (**D**) Raman spectra of the PTX IN PEG-AuNPs and DTX IN PEG-AuNPsproducts compared to free PTX and DTX as control. (**A-B**) Scale bars: 50 nm. (**D**)Raman spectra. Experimental conditions: λ_{exc} = 785 nm; laser power 20 mW; accumulation time 180s.

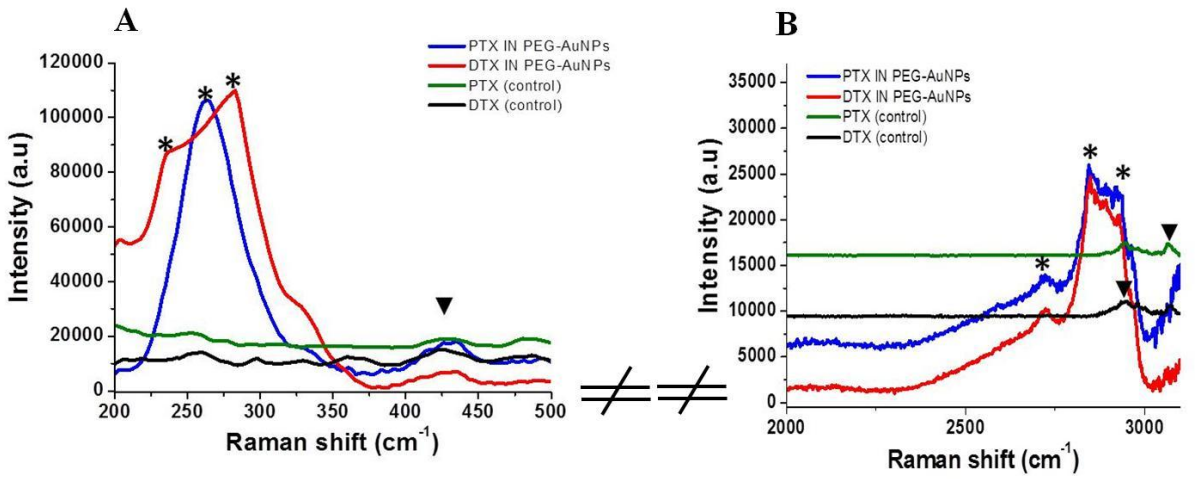

Figure 2. Raman spectra of the PTX IN PEG-AuNPs and DTX IN PEG-AuNPs compared to free PTX and DTX in the range 200-500 cm^{-1}(**A**) and 2000-3100cm^{-1}(**B**).Experimental conditions: λ_{exc} = 785 nm; laser power 20 mW; accumulation time 180 s.

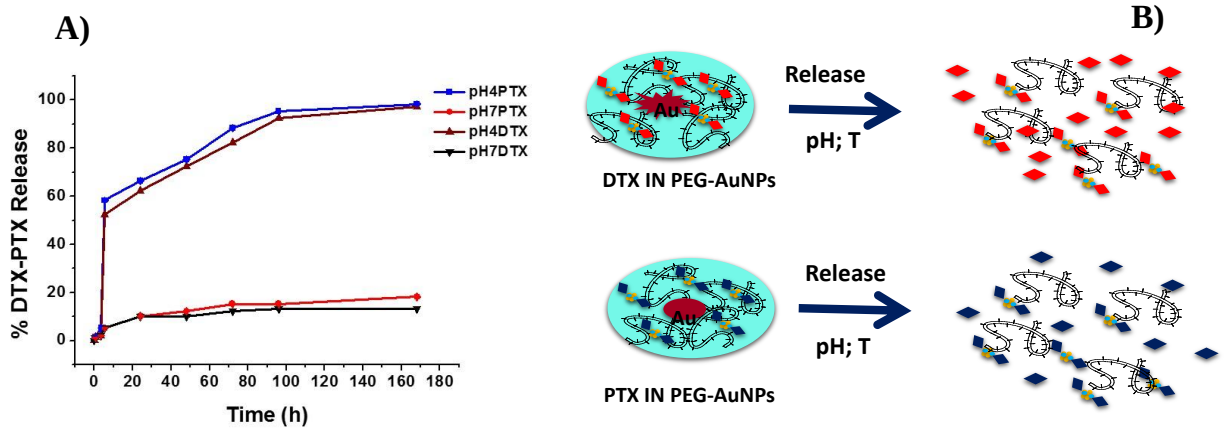

Figure 3: A) Drug release percentage (%) of DTX and PTX for DTX-IN-PEG-AuNPs and PTX-IN-PEG-AuNPs versus time in PBS (37 °C) at pH = 4.0 or at pH = 7.0. **B)** Schematic diagram of DTX and PTX release under pH conditions.

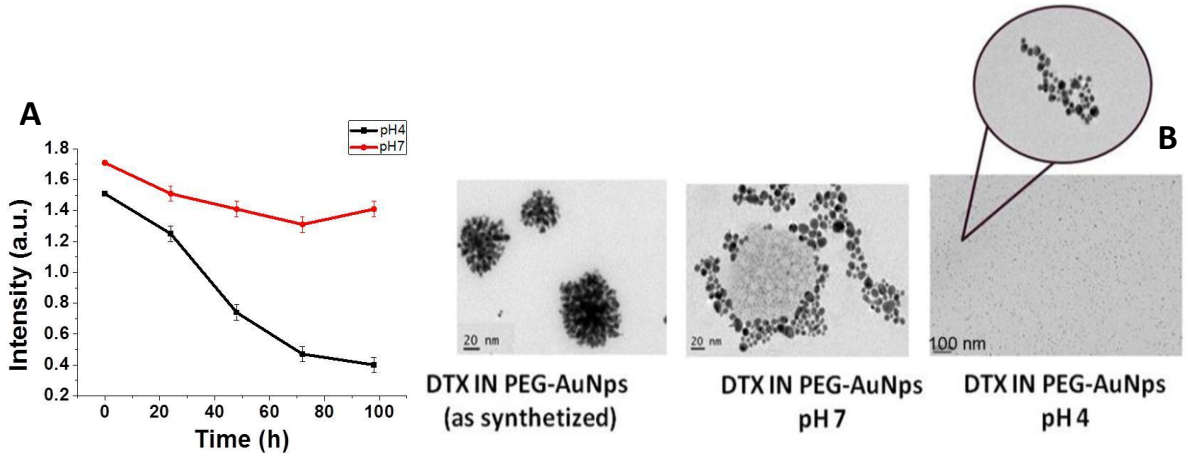

Figure 4:A) Variations of the Raman band intensity at 235-282 cm^{-1}versus time. DTX IN-PEG-AuNPs were incubated in PBS (37 °C) at pH 4.0 and pH 7.0 **B)** TEM images and conformational shape modifications under PBS (37 °C) at pH 4.0 and pH 7.0.

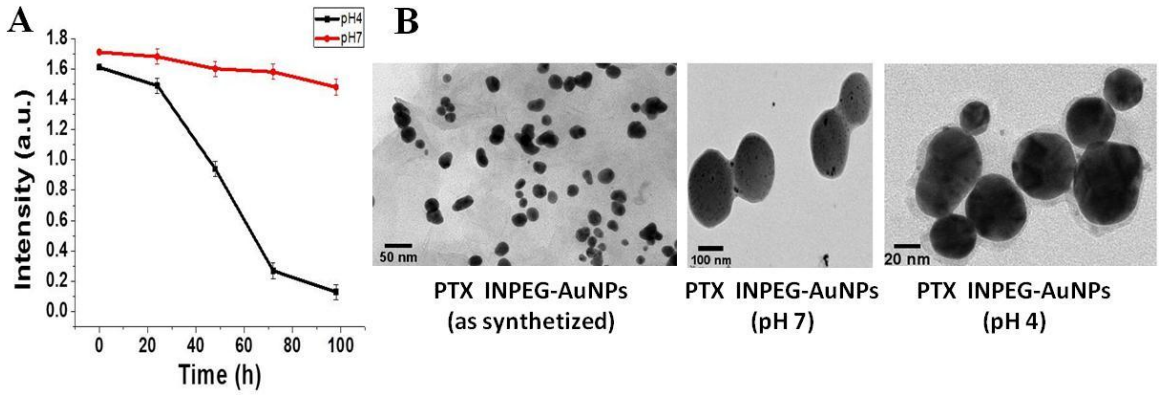

Figure 5:A) Variations of the Raman band intensity at 263 cm^{-1}versus time. PTX IN-PEG-AuNPs were incubated in PBS (37 °C) at pH 4.0 and pH 7.0 **B)** TEM images and conformational shape modifications under PBS (37 °C) at pH 4.0 and pH 7.0

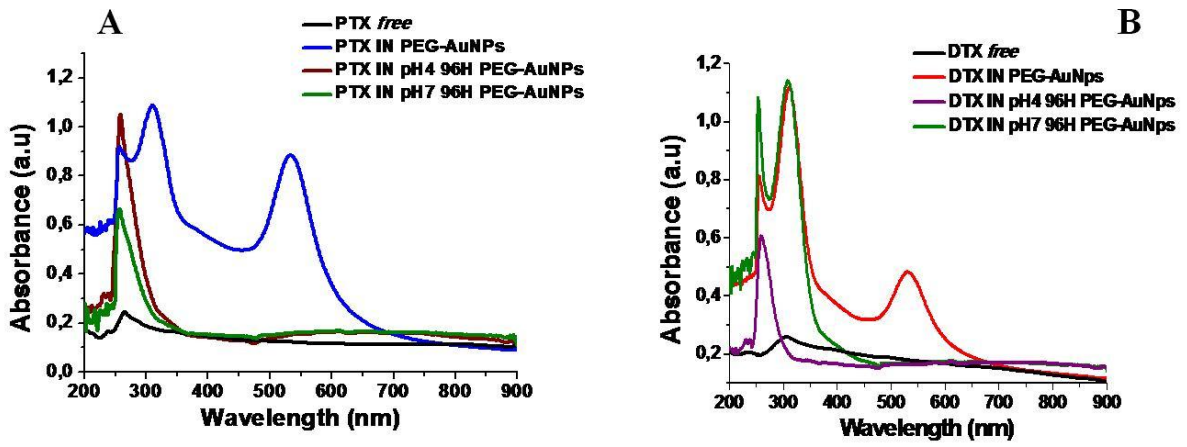

Figure 6: Drug Release (PTX; DTX) andchanges in theUV-Vis absorption spectra of PTX IN-PEG-AuNPs (panel A) and DTX IN-PEG-AuNPs when incubated in buffer solution at pH 7.0 and pH 4.0 up to 96h.

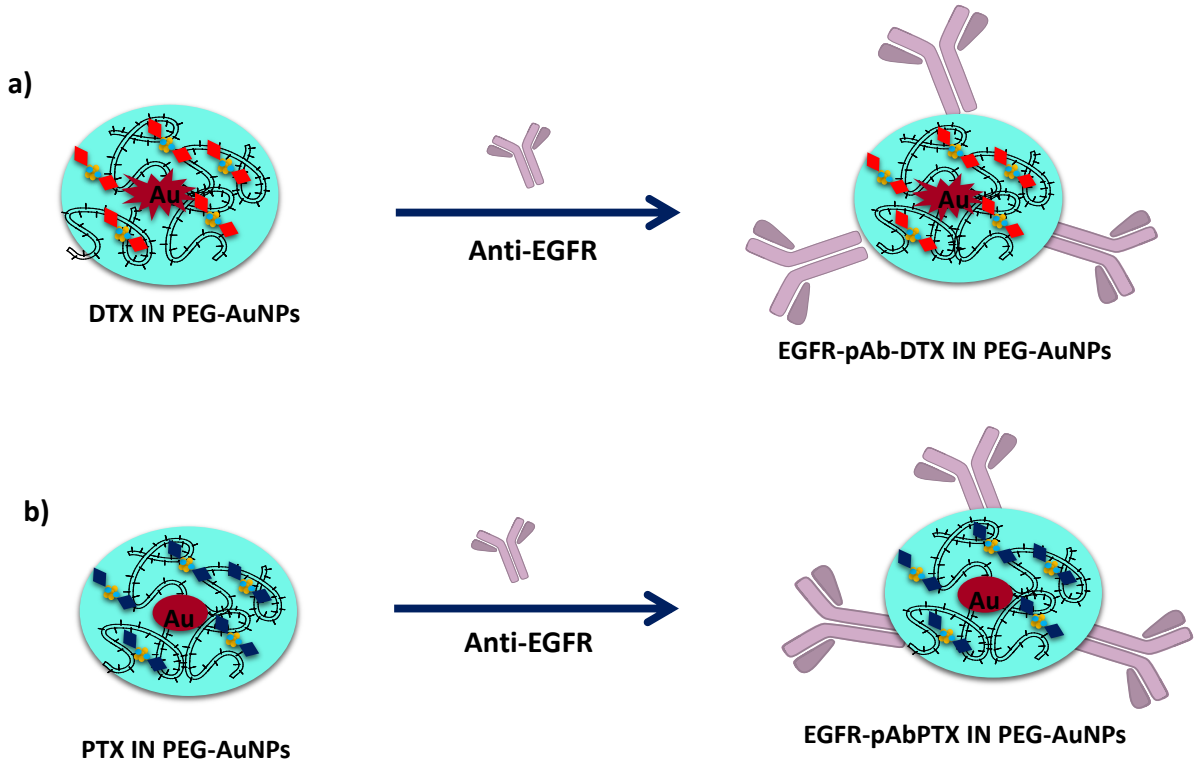

Scheme 2. Schematic representation of anti-EGFR-pAb bio-conjugating onto DTX IN-PEG-AuNPs (a) and PTX IN PEG AuNPs surface (b) (Please note that drawings are not in scale and are not intended as representative of the full samples composition).

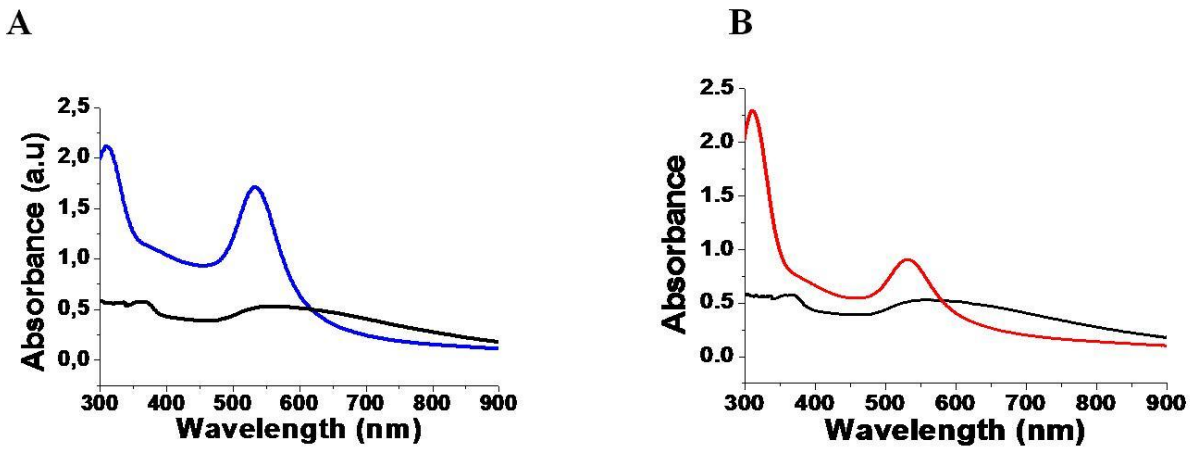

Figure 7: (A) Extinction spectra of PTX IN PEG-AuNPs before (blue line) and after conjugation to anti-EGFR-pAb (black line) and (B) DTX IN PEG-AuNPs before (red line) and after(black line) conjugation to anti-EGFR-pAb.

Supporting Information

Taxanes Hybrid Nanovectors: From design to physico-chemical evaluation of docetaxel and paclitaxel gold (III)-PEGylated complex –nanocarriers.

Gwendolyn Marguerit[1‡], Hanane Moustaoui[1‡], Maroua Ben Haddada[1], Nadia Djaker[1], Marc Lamy de la Chapelle[1], Jolanda Spadavecchia[1]*

[1] *CNRS, UMR 7244, CSPBAT, Laboratoire de Chimie, Structures et Propriétés de Biomateriaux et d'Agents Therapeutiques Université Paris 13, Sorbonne Paris Cité, Bobigny, France*

[2]*Southwest Hospital, Third Military Medical University, Chongqing, China*

* Corresponding author: jolanda.spadavecchia@univ-paris13.fr

- Supporting Information -

ADDITIONAL FIGURES

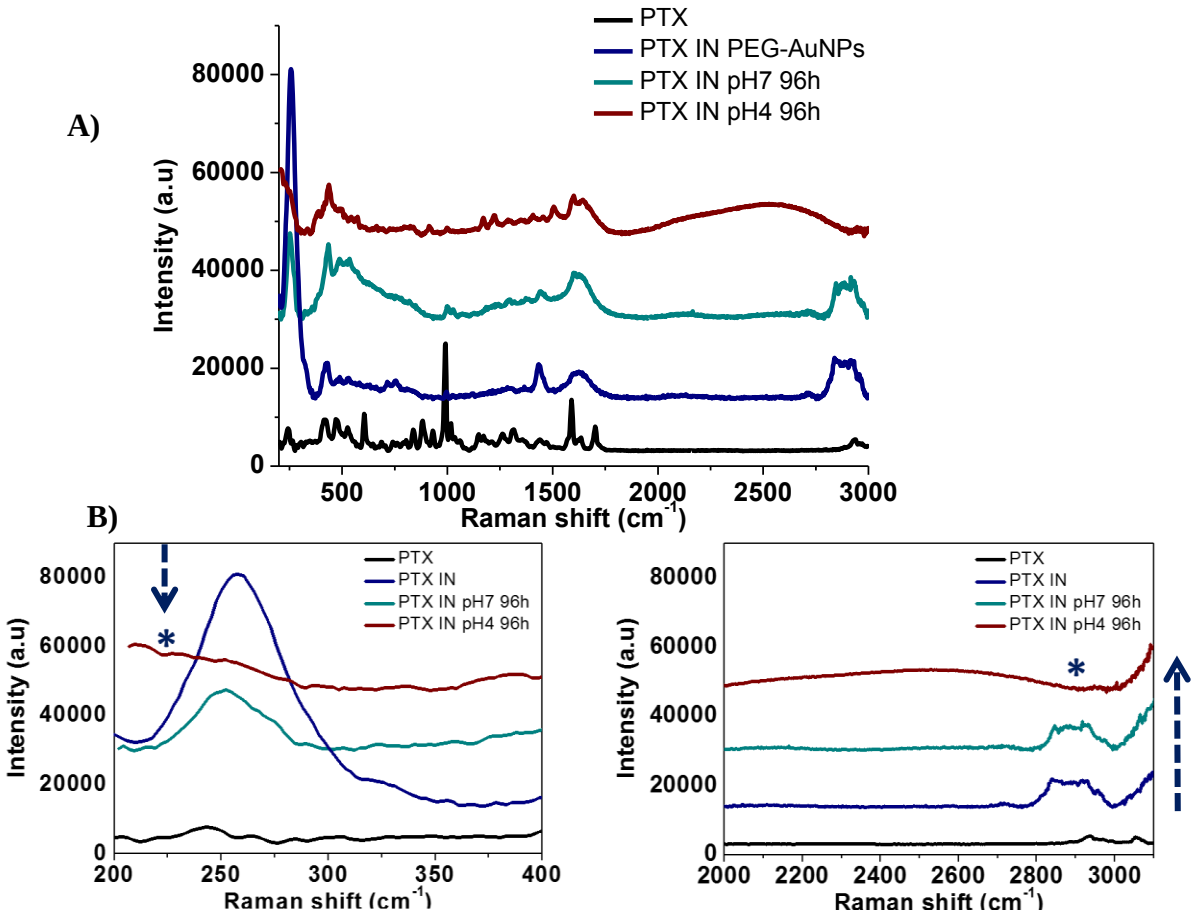

Figure S1: A) Raman spectra of PTX-IN-PEG-AuNPsbefore and after release of the PTX at pH 4.0 and pH 7.0 (time: 96 h).**B)** Raman spectra of PTX-IN-PEG-AuNPsbefore and after release of the PTX at pH 4.0 and pH 7.0 (time: 96 h).Experimental conditions: λ_{exc} = 785nm; laser power 20 mW; accumulation time: 180 s**.**

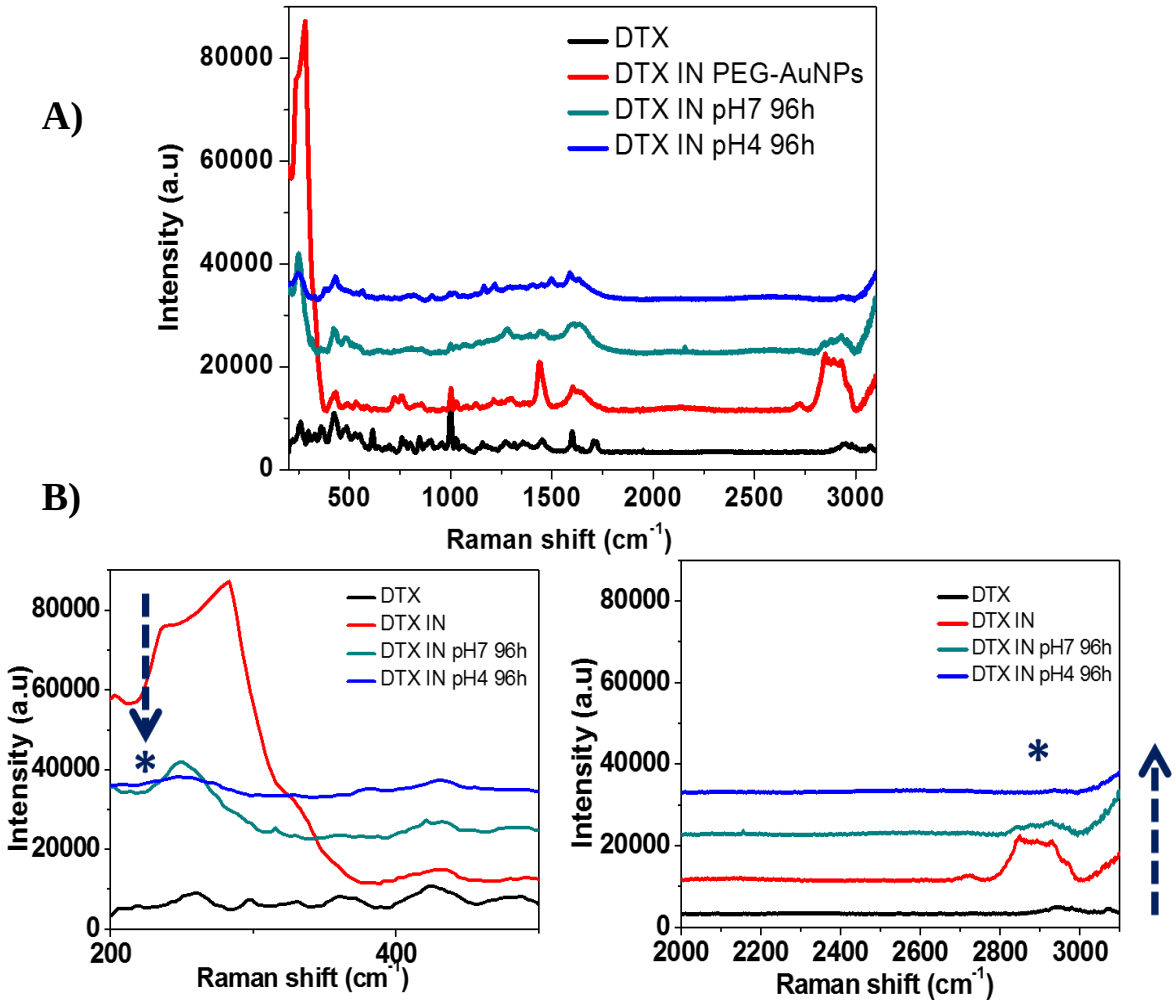

Figure S2: A) Raman spectra of DTX-IN-PEG-AuNPsbefore and after release of the DTX at pH 4.0 and pH 7.0 (time: 96 h).**B)** Raman spectra of DTX-IN-PEG-AuNPsbefore and after release of the DTX at pH 4.0 and pH 7.0 (time: 96 h).Experimental conditions: λ_{exc} = 785nm; laser power 20 mW; accumulation time: 180 s**.**

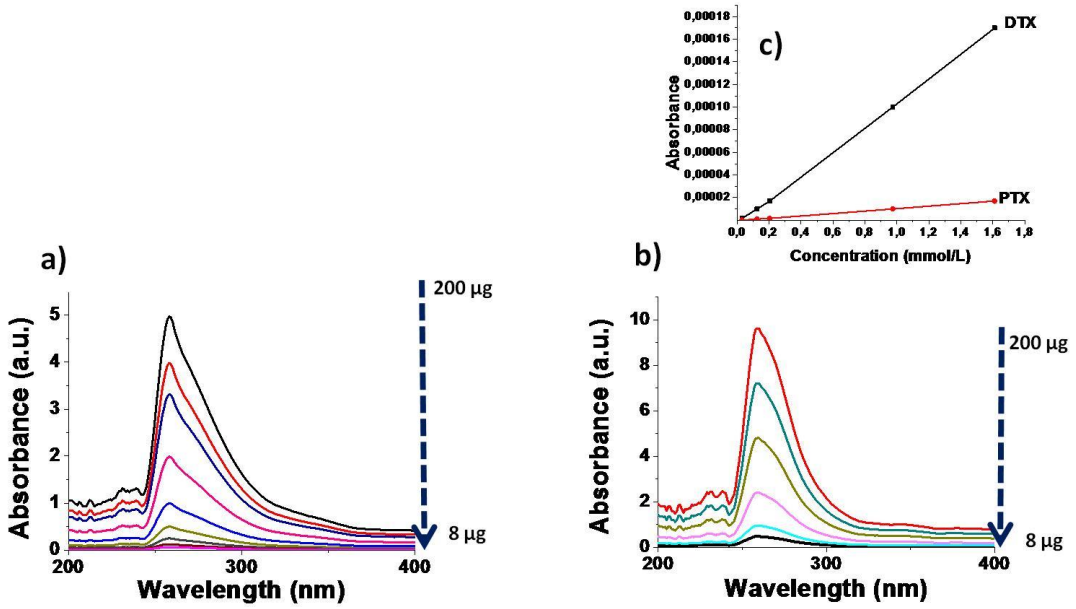

Figure S3: UV-Vis absorption spectra of (a) PTX or (b) DTX at increasing known concentrations. (c) Calibration curve extrapolated from such measurements. The amount of PTX or DTX molecules contained into PTX IN-PEG-AuNPs or DTX IN-PEG-AuNPs, respectively, was estimated based on this curve.

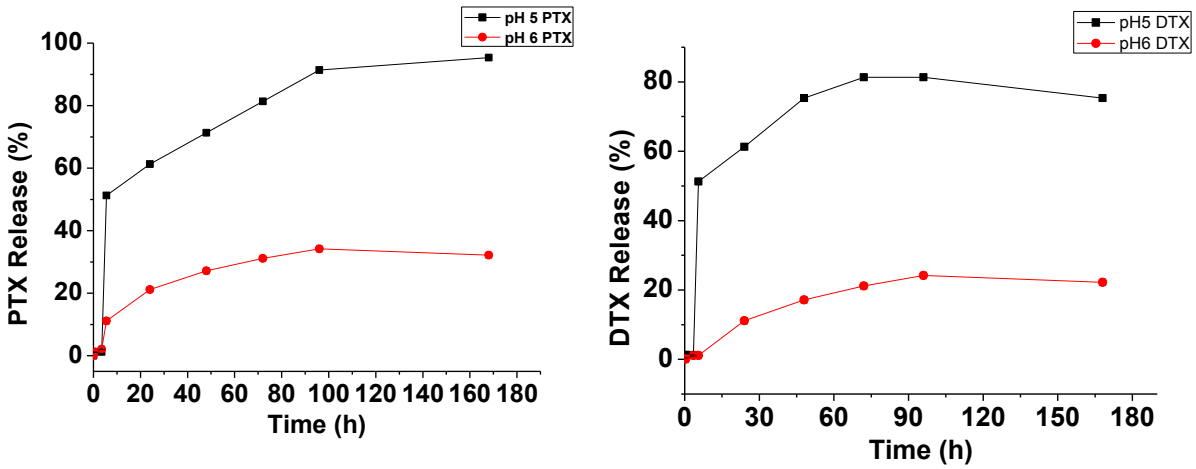

Figure S4: Drug release percentage (%) of PTX and DTX for PTX-IN-PEG-AuNPs (*left graph*) and DTX-IN-PEG-AuNPs (*right* graph) versus time in PBS (37 °C) at pH = 5.0 or at pH = 6.0.

Test Stability:

Stability of DTX (PTX) IN PEG AuNPs as function of pH

DTX (PTX) IN PEG AuNPs were exposed to different pH solutions in order to understand the behaviour of nanoparticles as further drug-deivery tools.

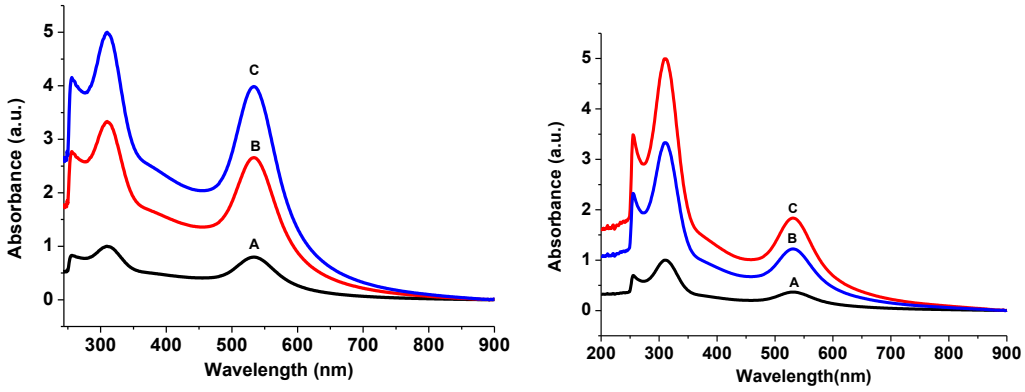

UV-Vis spectra of DTX (PTX) IN PEG AuNPs in buffer solutions at pH 1.68 (A), 7 (B) and 12.45 (C).

So as, DTX (PTX) IN PEG AuNPs were exposed to buffer solution at three different pH (1.68, 7 and 12.45) and the interaction was carried out for 18h. Figure S1 showed UV Vis spectra of DTX (PTX) IN PEG AuNPs with typical peak at 280nm and the nanoparticles topic peak at 535nm for PTX IN PEG AuNPs (spectra left) and 533nm for DTX IN PEG AuNPs (spectra right) . In conclusion, present investigation reveals the ability of PEG-HFB-AuNPs to interact with from buffer solution at different pH maintaining unchanged absorbance during 18h.

ADDITIONAL TABLES

Table S1. Assignment of experimental Raman bands of PTX IN PEG-AuNPs and DTX IN PEG-AuNPs and their assignementto possible vibrational modes in the range spectral 200-4000 cm^{-1}.

PTX Raman (cm^{-1})	DTX Raman (cm^{-1})	PTX IN-PEG-AuNPs (cm^{-1})	DTX ON-PEG-AuNPs (cm^{-1})	Bands assignment (cm^{-1})
---	---	263 (single peak)	235-282(double peak)	ν(AuCl), δ(OAuO)
431	431	431	431	δ(OH…O), ν(OH…O) (PEG), δRing (Phe), ωC-H. νC-H (PEG)
536	536	536	536	δ(OH…O), ν(OH…O) (PEG), δRing (Phe), ωC-H. νC-H (PEG),
613	616	---	---	δ(OH…O)
---	---	721-761 (double peak)	724-758 (double peak)	ω N-H, δ (Ring)
1001	1001	1001	1001	δ (CC=O), δ (COC)
1445	1445	1439 (strong peak)	1439 (strong peak)	δRing (Phe), ν(C=C), ν(C=O), δ(OAuO)
1600	1600	1600	1600	ν(C=C), ν(C=O), δRing (Phe),
1714	1711	---	---	ν(C=O) nalidixic acid
2946	2952	---	---	CH_3/C-H stretching
---	---	2847-2889-2929 (Triple peak)	2847-2889-2929 (Triple peak)	C-C/CH_3 (PEG)
---	---	2720 (single peak)	2720 (single peak)	C-H (PEG)
3068	3068	---	---	Ar-CH stretching , υ N-H